ISSN 2029-6991 / eISSN 2029-7009

VILNIUS TECH
Vilnius Gediminas Technical University

GEODESY and CARTOGRAPHY

2025
Volume 51
Issue 3
Pages 131–140
https://doi.org/10.3846/gac.2025.19884

UDC 528.873

INTEGRATED INDEX ANALYSIS FOR MONITORING URBAN GROWTH BASED ON GIS AND REMOTE SENSING DATA IN KARBALA PROVINCE, IRAQ

Nabaa Falih NASER✉, Israa Fadhil IBRAHEEM, Mufid AlHADITHI

Technical Engineering College, Middle Technical University, Baghdad, Iraq

Article History:
- received 08 August 2023
- accepted 29 August 2024

Abstract. Remote sensing techniques and GIS were used in this study to monitor urban growth in Karbala Governorate, Iraq. A compiled database was created from available Multi-temporal Landsat (TM, ETM+ and OLI) data from 2000 to 2018. The near infrared (NIR), visible red (R), and short infrared (SWIR) wavelength areas covered by Landsat bands have been used to generate spectral indices known as the Normalized Difference Built-Up Index (NDBI), Normalized Difference Vegetation Index (NDVI), Normalized Difference Water Index (NDWI) and Normalized Difference Salinity Index (NDSI). Images of the Landsat 7 and 8 satellites that were free to download from the USGS website between the years of 2000 and 2018 were the data used in this study. The layers were classified and merged to reveal the dynamic changes of land cover in the study area. The result shows that the built-up area increased from 264.75 km^2 in 2000 to 391.23 km^2 in 2018, indicating an increase over 18 years, but over the same period, the amount of water decreased.

Keywords: GIS, urban growth, Remote Sensing Landsat, spectral indices, NDVI.

✉Corresponding author. E-mail: ***nabaatcb@mtu.edu.iq***

1. Introduction

Urban development, especially the expansion of domestic and business land use outside of urban centers, has long been seen as an indication of the health of the local economy. However, its advantages are increasingly outweighed by its negative effects on the environment, such as the deterioration of air and water pollution and the loss of farms and woodlands, as well as its negative socioeconomic effects, such as economic disparities, social fragmentation, and infrastructure costs (Ibraheem, 2022; Squires, 2002).

Urban sprawl is the term for land changes brought on by the quick growth of low-density neighborhoods into formerly agricultural regions and Exurbs, or metropolitan or suburban regions separated from one another by undeveloped territory, have an impact on the socioeconomic and natural viability of communities. Urban sprawl is the word for unplanned urban development in a city's suburbs which is on the rise as a result of the population's constant growth (Bugliarello, 2003; Ibraheem & Al-Hadithi, 2024; Theobald, 2001). It is an unplanned, uneven pattern of development that is fueled by various processes and ultimately results in inefficient resource, so utilization urban growth management is essential to stopping a city's ongoing expansion (Bhatta et al., 2010).

The trend mentioned focuses on land use and frequently portrays it incorrectly because it is based on traditional land surveys conducted by administration officials (Naser et al., 2025). The amount of greenery in urban regions is being negatively impacted by the rate of urbanization. Due to the increased desire for development in urban areas worldwide since the 20th century, the amount of green areas has been declining (Kaufmann et al., 2007; Melesse et al., 2007; Weng, 2007; Xian & Crane, 2006; Xu, 2008). In urban, suburban and agricultural research, determining the location, size and distribution of the built-up area is very important. Remote sensing and multispectral space and series intertemporal satellite images offer trustworthy scientific instruments for calculating the built-up area and utilizing. In comparison to traditional ground trothing techniques used to map and monitor urban growth the remote sensing has a number of advantages where it has been used at the regional, local, and temporal stages in several studies (Boori et al., 2015; Griffiths et al., 2010).

Remote sensing images are helpful for tracking the spatial distribution and growth of urban metropolitan areas because they can provide thorough and timely views of land cover (Griffiths et al., 2010; Guindon et al., 2004; Ibraheem, 2023; Xu, 2008). The normalized difference built-up index (NDBI) allows for the automatic mapping of built-up urban areas (Zha et al., 2003). The approach benefits from the distinct spectral responses of populated regions and other land covers. The successfully constructed regions are mapped using a mathematical modification of the NDVI and NDBI images generated were re-encoded from the Landsat Thematic Mapper (TM) images. The method developed using the assumption that a positive value of NDBI should indicate built-up areas and a positive value of NDVI should indicate undeveloped areas, re-encoding the resulting NDBI and NDVI images to generate binary images (Zha et al., 2003). This study has been conducted with the goal of this research is to Combine (NDVI) and (NDBI) indices for monitoring Urban Growth trend in Karbala Province, Iraq using multitemporal satellite data for the period 2000 to 2018. The research includes the following paragraphs: 1 – Introduction, 2 – Materials and methods, 3 – Methodology, 4 – Result and discussion, 5 – Conclusions.

2. Materials and methods

2.1. Study area

Karbala is located to the south of the capital Baghdad about 105 km away from it, and the city rises 30 meters above sea level. It is located in an important location that connects it to the Saudi Arabia borders through Al-Nukhaib, from the north it is connected to the capital, Baghdad, from the south it is connected to Najaf, and from the southeast side to Hila. The area of Karbala is (5031) km^2. The city is located at longitude 44° 42′ and latitude 33° 31′ as shown in Figure 1.

2.2. Data used

The data used in this study are images of Landsat 7 and 8 satellites downloaded from the USGS web page for free from 2000 to 2018 Table 1. Images from the Landsat satellite at 30*30 pixels were used because higher resolution is not available except for a price, since 2006, high-resolution images of the region began to be available. In future research, we will use satellite images with higher resolution.

Table 1. Landsat 7 Enhanced Thematic Mapper plus (ETM+)

Band	Wavelength (micrometers)	Resolution (meters)
Band 1-Blue	0.45–0.52	30
Band 2-Green	0.52–0.60	30
Band 3-Red	0.63–0.69	30
Band 4-Near Infrared (NIR)	0.77–0.90	30
Band 5-ShortWave Infrared (SWIR)1	1.55–1.75	30
Band 6-Thermal	10.40–12.50	60*(30)
Band 7-ShortWave Infrared (SWIR)2	2.09–2.35	30
Band 8-Panchromatic	0.52–0.90	15

The operational land imager (OLI) and thermal infrared (TIRS) are two of the sensors on board these satellites. Except for the panchromatic band, the OLI sensor contains nine bands with a spatial resolution of 30 m, and the TIR sensor has two thermal bands with a 100 m spatial resolution as shown in Table 2.

Mosaicking and subset process by ERDAS imagine 2014 and then open it in the GIS program, which is a process of compiling satellite images to form a single compound (Figure 2).

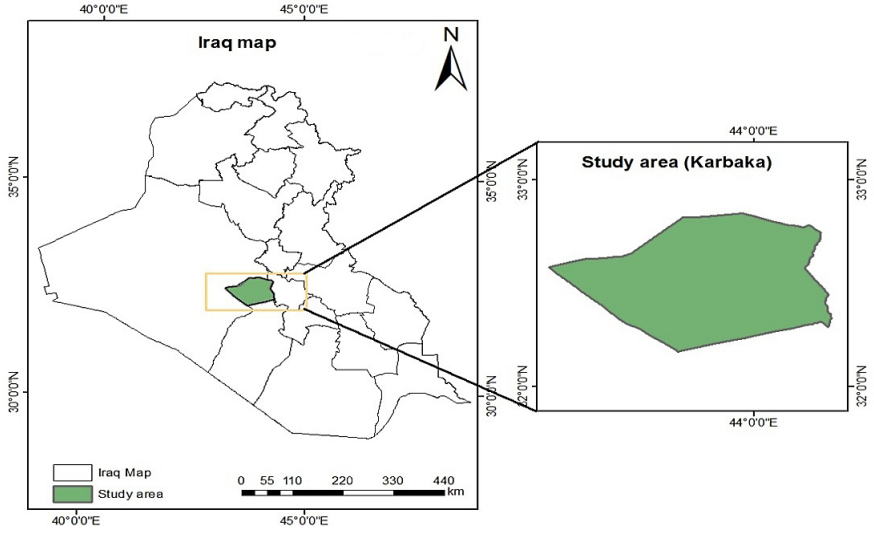

Figure 1. Location map of the study area

Table 2. The band characteristic for Landsat 8 (source: Acharya & Yang, 2015)

Band	Wavelength (micrometers)	Resolution (meters)
Band 1-Ultra Blue (coastal/aerosol)	0.435–0.451	30
Band 2-Blue	0.452–0.512	30
Band 3-Green	0.533–0.590	30
Band 4-Red	0.636–0.673	30
Band 5-Near Infrared (NIR)	0.851–0.0.879	30
Band 6-Shortwave Infrared (SWIR)1	1.566–1.651	30
Band 7-Shortwave Infrared (SWIR)2	2.107–2.294	30
Band 8-Panchromatic	0.503–0.676	15
Band 9-Cirrus	1.363–1.384	30
Band 10-Thermal Infrared (1)	10.60–11.19	30
Band 11-Thermal Infrared (2)	11.50–12.51	30

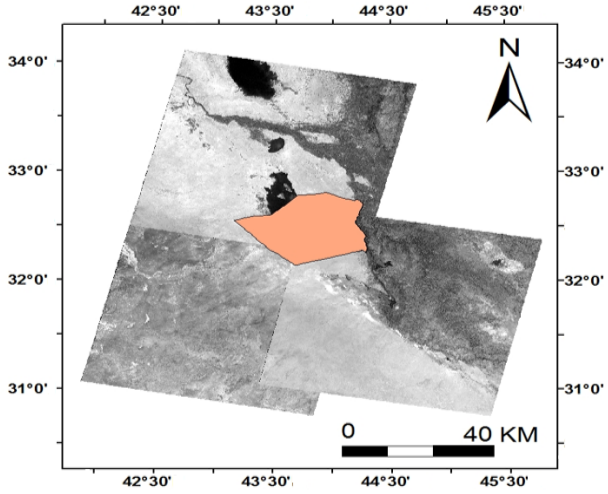

Figure 2. Image mosaic and subset process

3. Methodology

3.1. Pre-processing images

ArcGIS 10.3 has been used to process images. Floats are processed both visually and digitally. The entire study area was mapped using shape files.

3.2. Analyzing image

NDVI index was calculated using ArcGIS 10.3, and the work steps were as shown in Figure 3.

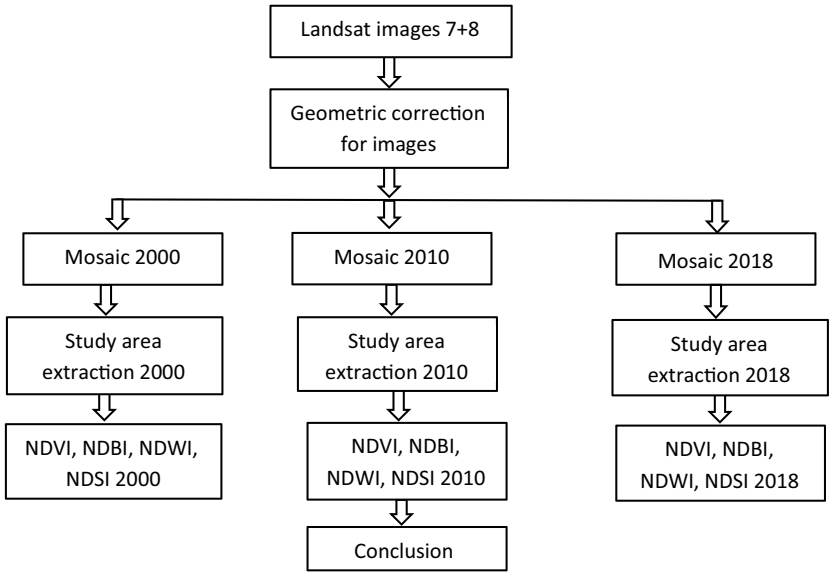

Figure 3. Methodology flowchart

3.3. Spectral indexes

The following steps explain the work steps in precise detail.

3.3.1. Normalized Difference Vegetation Index (NDVI)

NDVI is generated from remote sensing (satellite) data as it is closely related to drought conditions. It is based on measuring the intensity of green on a plot of land using different colors (wavelengths) of visible and near-infrared sunlight reflected by plants. The red and near infrared bands were used to calculate the NDVI. Estimating the NDVI index, which represents the amount of vegetation cover, is important and a key factor for estimating the general vegetation status in the region.

The near-infrared and red reflectance differences of green vegetation were used to compute NDVI. The Equation (1) was used to determine the *NDVI* (Archarya & Yang, 2015):

$$NDVI = \frac{(NIR - RED)}{(NIR + RED)}. \quad (1)$$

The value of NDVI ranged from –1 to 1, when it is equal to 1 indicates a high density of vegetation and –1 indicates a low density of vegetation and zero means that the land is barren. All obtained values have been transferred to GIS environments and thematic map of NDVI index have been created for the period of 2000, 2010 and 2018 as shown in Figure 4.

3.3.2. Normalized Difference Built-up Index (NDBI)

It is a digital index that is created using remote sensing by examining the electromagnetic energy of near-infrared (NIR) and shortwave infrared (SWIR) radiation. It is predicted on the idea that the urban environment is a complex ecosystem made up of four primary elements: the soil, the water bodies, the green flora, and the surface material. In satellite images, NDBI employs wavelengths and is rendered as layers for use in metropolitan areas (Al-Dabbas & Manii, 2009).

$$NDBI = \frac{(SWIR - NIR)}{SWIR + NIR)}. \quad (2)$$

The values of NDBI range from (+1 to –1) a number near to +1 denotes the presence of built-up areas, whereas a value close to –1 denotes the absence of built-up regions. The obtained results values were transferred to GIS environments for the purpose of creating a thematic map of NDBI for the periods 2000, 2010 and 2018 as shown in Figure 5.

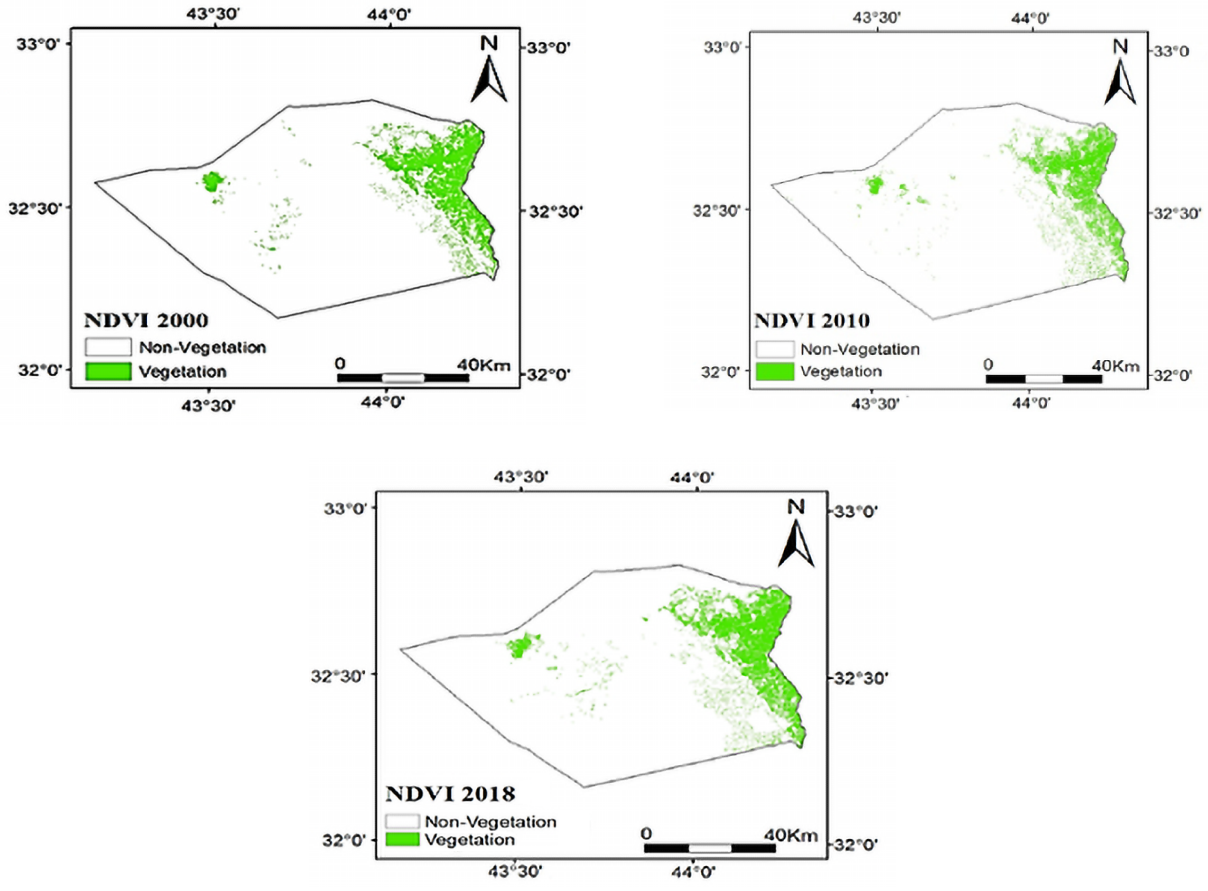

Figure 4. NDVI for the year 2000, 2010 and 2018

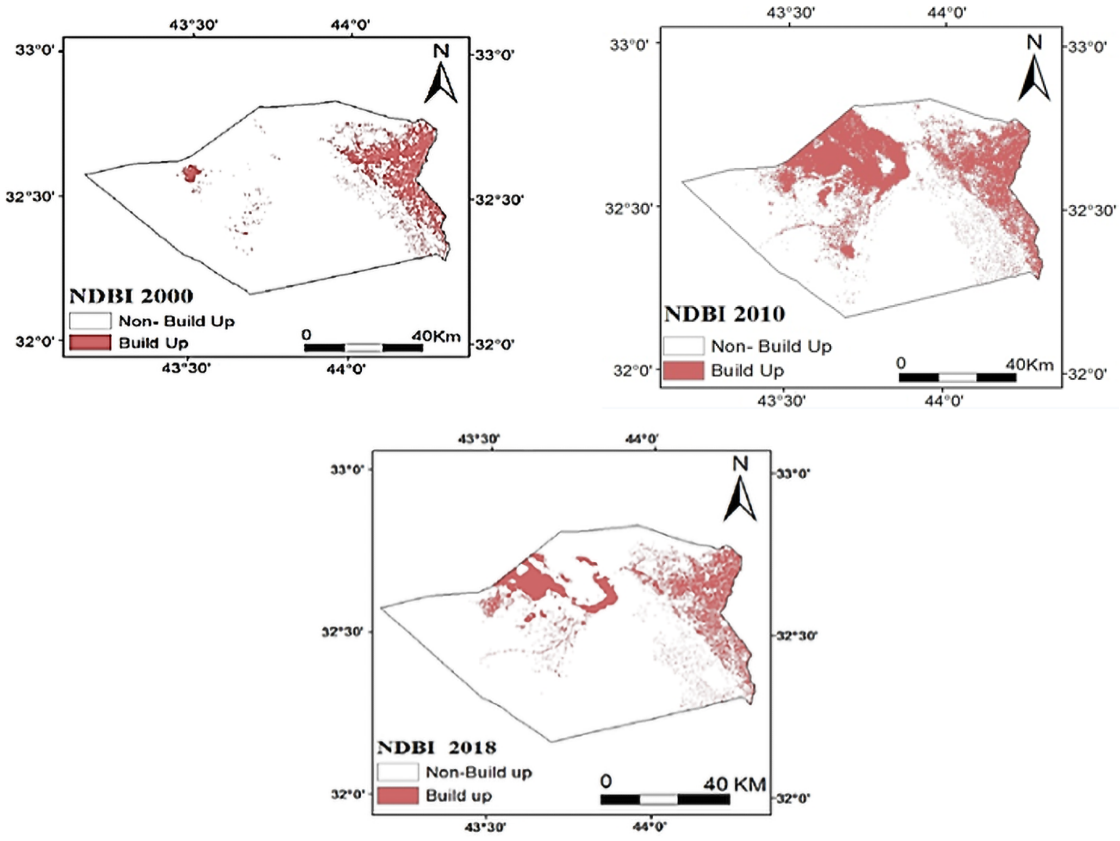

Figure 5. NDBI for the year 2000, 2010 and 2018

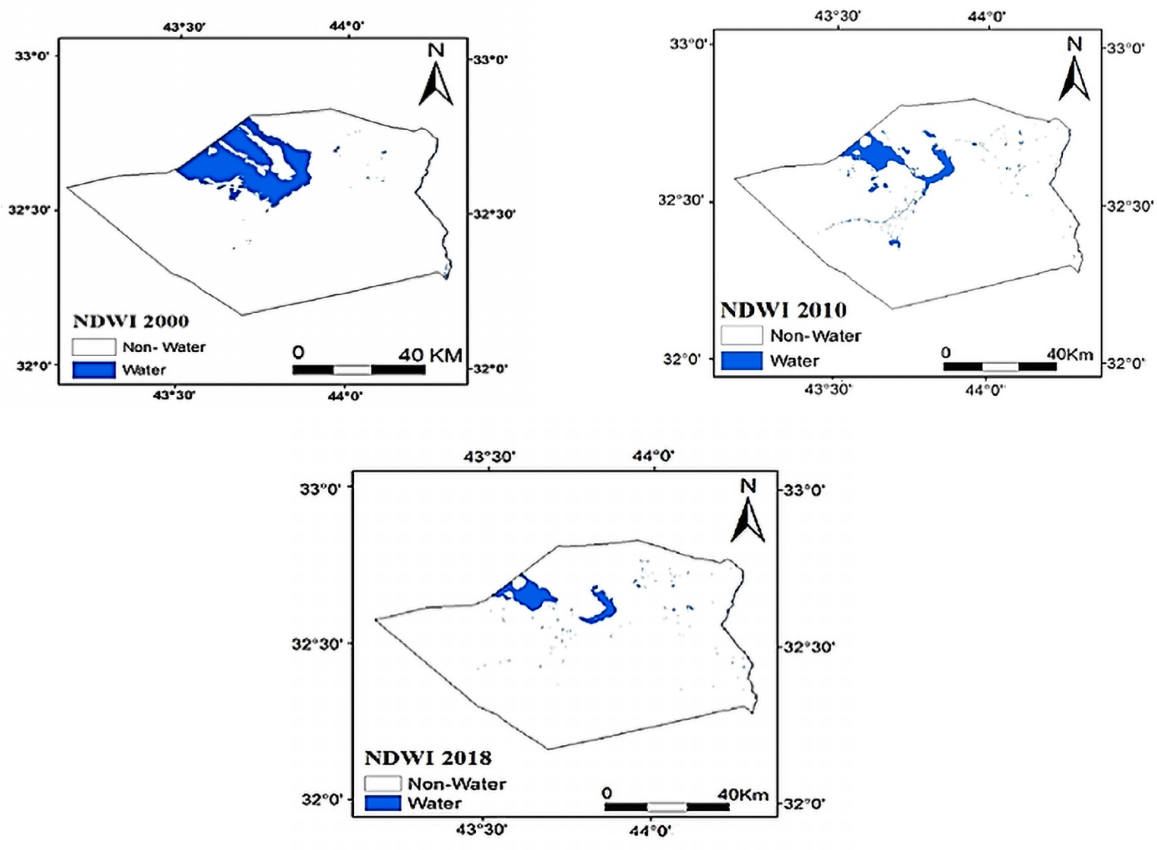

Figure 6. NDWI for the year 2000, 2010 and 2018

3.3.3. Normalized Difference Water Index (NDWI)

It is a new, advanced technique designed to identify the characteristics of open water areas, recognize different wetlands, and gauge the volume of surface water. To distinguish between land and water, this is accomplished utilizing remote sensing data and the NDWI ratio. Normalized Difference Water index (NDWI) was calculated from data of the related Landsat bands of TM, ETM and OLI within the periods of 2000, 2010 and 2018 respectively, using the Equation (3):

$$NDWI = \frac{Green - NIR}{Green + NIR}. \quad (3)$$

If the values of NDWI are smaller than zero or equal to zero, this indicates the non-water bodies, but if the values are greater than zero, they represent the water bodies. The obtained values are transferred into the GIS environment for the purpose of creating thematic maps for the period of 2000, 2010 and 2018 as shown Figure 6. The urban surface water bodies were extracted by Normalized Difference Water Index (NDWI) from Landsat satellite. The images were then classified into two categories consisting of water and non-water objects. Furthermore, water areas have values greater than zero while vegetation and urban areas have negative values. The urban water body was extracted by Modified Normalized Difference Water Body because this method is more suitable for increasing the accuracy of water extraction and effectively reduce as well as remove built-up land noise than NDWI. Furthermore, MNDWI can be concluded in more detail detecting urban water surface than NDWI (Ali et al., 2019).

3.3.4. Normalized Difference Salinity Index (NDSI)

In agricultural settings, salinization–the process of enhancing soil with soluble salts and producing information about salt-impacted soil–is a type of land degradation (Zhao & Chen, 2005).

A typical cause of salinity in irrigated soils is the build-up of soluble salts brought on by regular irrigation with water that has a high or moderate amount of dissolved salts which is calculated using the Equation (4):

$$NDSI = \frac{(R - NIR)}{(R + NIR)}. \quad (4)$$

All results were transferred to GIS environment to produce the thematic map of NDSI maps detect the changes for three periods 2000, 2010 and 2018 as shown in Figure 7.

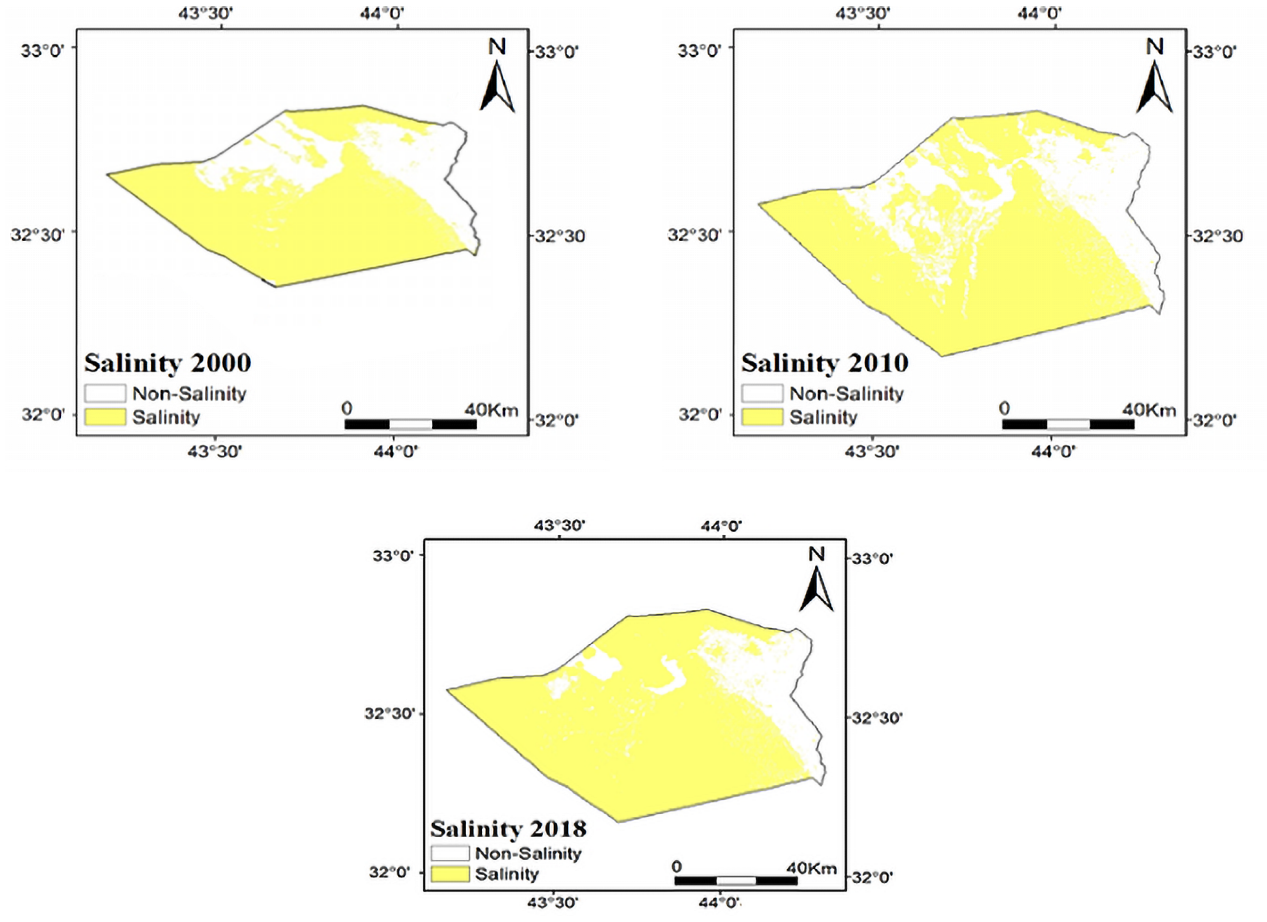

Figure 7. NDSI for the year 2000, 2010 and 2018

4. Result and discussion

Thematic maps were created for a number of indicators using the geographic information systems environment for the purpose of monitoring the trend of urban growth in Karbala Governorate, Iraq, which have been conducted by determining the amount of changes that occurred in these indicators and thus determining the area under study's rate of change. The details of the different LULC maps are discussed below for the purpose of knowing the changes in these indicators in the study area.

4.1. Classification

Both supervised and unsupervised classifications have been heavily used in numerous previous studies to produce classifier maps and final output analysis. Most supervised case classifications have been found to be more accurate (Erol & Akdeniz, 1998). Supervised classification was used in this study, and 40 samples were taken for each class have been used for model training. This classification approach stands out for its high accuracy, very low error rate, speedy region classification, and area computation for every recognized.

Supervised classification was used in this study. To illustrate the changes in land use seen in the maps made for the years 2000, 2010, and 2018, the area was divided into four main classes based on the satellite images (Figure 8). These groups include built-up areas, barren land, vegetation, and water bodies. The kappa coefficient and overall accuracy were utilized to evaluate the classifications' accuracy (Qin & Karnieli, 1999; Schmugge et al., 2002). The percentages were, in order, 91.1%, 90%, and 94.2%. Google Earth has been used to compare the "ground truth" Class type of the 45 reference points from 2000, the 40 reference points from 2010, and the 35 reference points from 2018 with the various land use categories that they were chosen to represent. The calculated overall accuracy (94.2%) is greater than the 90% and 91.1% Kappa values. Variations among these metrics are anticipated, given that they incorporate distinct types of data from the error matrix. The overall accuracy only takes into account data along the principal diagonal; errors by commission and omission are not included. However, a row and column marginal product is included to represent the nondiagonal components of the error matrix as displayed in Tables 3, 4, and 5.

$$\text{overall accuracy} = \text{TCS (diagonal)}/\text{TS} \times 100; \quad (5)$$

$$\text{kappa coefficient (T)} = (\text{TS} \times \text{TCS}) - \text{S(Column total} \times \text{Row total)/TS2} - \text{S(Column total} - \text{Row total)} \times 100, \quad (6)$$

where: TS – Total number of reference pixels; TCS – Total number of correctly classified pixels.

Table 3. Accuracy assessment using the selected reference pixels in 2000

Classification	Water	Barren land	Vegetation	Built up area	Total (User)
Water	10	0	0	0	10
Barren land	0	10	0	0	10
Vegetation	0	3	8	1	12
Built up area	0	0	0	13	13
Total producer	10	13	8	14	45

Table 4. Accuracy assessment using the selected reference pixels in 2010

Classification	Water	Barren land	Vegetation	Built up area	Total (User)
Water	10	0	0	0	10
Barren land	0	10	0	0	10
Vegetation	0	0	10	0	10
Built up area	0	2	2	6	10
Total producer	10	12	12	6	40

Table 5. Accuracy assessment using the selected reference pixels in 2018

Classification	Water	Barren land	Vegetation	Built up area	Total (User)
Water	11	0	0	0	11
Barren land	0	9	0	0	9
Vegetation	0	1	5	1	7
Built up area	0	0	0	8	8
Total producer	11	10	5	9	45

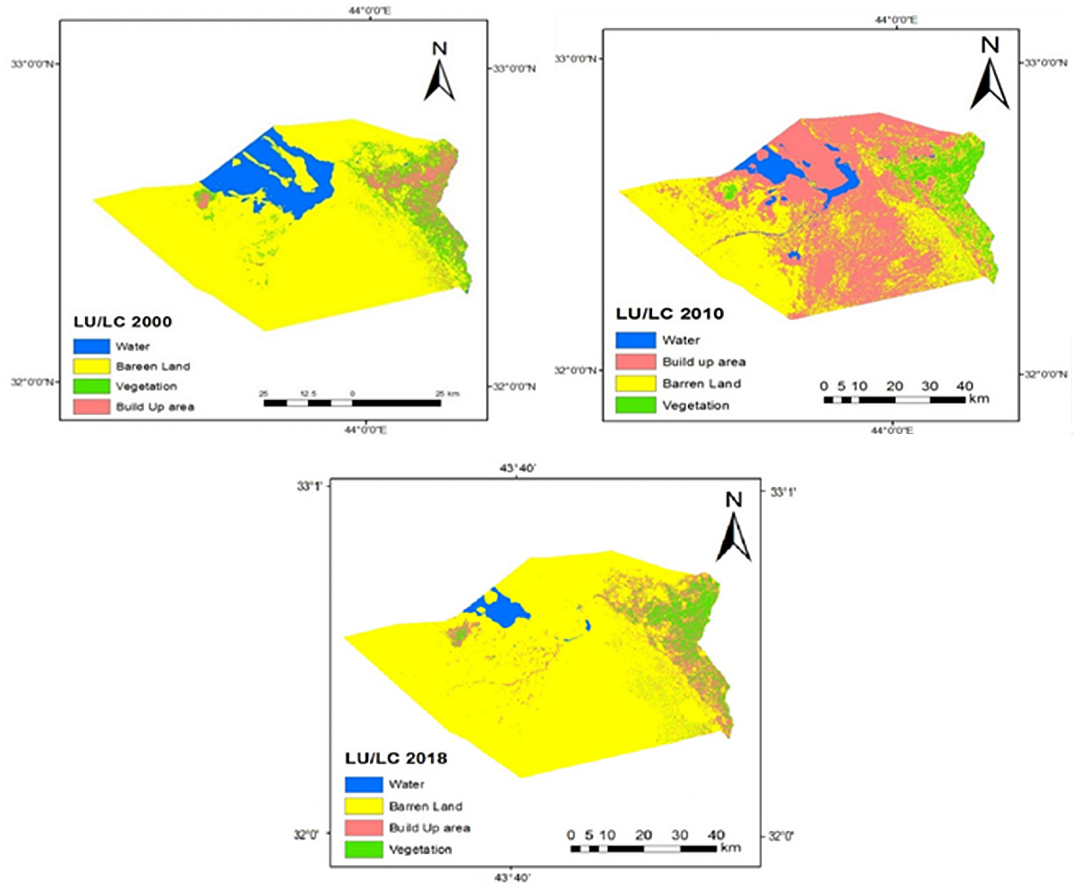

Figure 8. Supervised classification for the study area for the period 2000, 2010 and 2018

4.2. Land use/land cover change detection

It is the process of extracting information by comparing two or more images of an area obtained at different times that provide important information about the resource at risk. It has been widely used to evaluate changing agriculture, deforestation, urban growth, impact of natural disasters, earthquakes, land use/land cover changes etc. It was renowned that the changing rate in spectral indices such as NDVI, NDWI, NDBI, and NDSI were negative between the years 2000–2010 while the changes in NDBI and NDSI between the years 2000–2018 became positive (Table 6).

The changes in NDVI and NDWI were negative in the same period as shown in Table 6. The NDVI and NDWI results show that built-up areas and water areas were high during 2000, decreased during 2010, and decreased

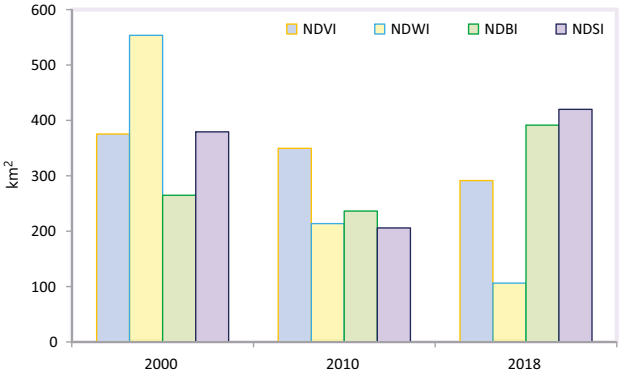

Figure 9. Changes in land cover in Karbala over the period of 2000, 2010 and 2018

Table 6. Areas of spectral indices (NDVI, NDWI, NDBI and NDSI)

Land cover class	2000	2010	2018	Changes (km^2)	
	Area (km^2)	Area (km^2)	Area (km^2)	2000–2010	2000–2018
NDVI	375.21	349.43	291.37	–25.78	–83.84
NDWI	553.45	213.50	106.07	–339.95	–447.38
NDBI	264.75	236.46	391.23	–28.29	126.48
NDSI	379.26	205.84	419.73	–173.42	40.47

significantly in 2018, while both NDBI was low in 2000, decreased over 2010, and then increased significantly in 2018 (Figure 9). It is noted also that the NDSI ratio was significantly high in 2000, then decreased in 2010. It then greatly increased in 2018, as a result of the research area's high rate of desertification, rising salinity, and high temperatures. This area has been severely affected by factors including lack of water resources, increased soil salinity and loss of vegetation cover. The results showed, according to the maps, that the areas with a high salinity percentage began to increase from the center, west, and south of Karbala governorate areas. As we approached the areas east of the city, the population density increased, the amount of green space increased as a result of rain and an abundance of water cover, and the salinity rate reduced.

5. Conclusions

Multitemporal Remote Sensing Satellite data from the previous 18 years were used to track the growth of the current research region in the province of Karbala. Landsat TM, ETM+, and OLI multitemporal data from 2000 to 2018. Different spectral indices, such as the Vegetation Index (NDVI), Normalized Difference Built-Up Index (NDBI), Normalized Difference Water Index (NDWI), and Standard Difference Salinity Index (NDSI), are employed to specify and define urban expansion zones and other types of urban cover. The main conclusions of the present study can be summarized as follows:

1. The NDVI map results indicate that the vegetation cover decreased between the years 2000 and 2018 from 375.21 km^2 to 291.37 km^2 as a result of an increase in building area and the conversion of agricultural land to residential land.
2. As a consequence of climate change, high temperatures, and a lack of precipitation, the study area's water area decreased from 553.45 km^2 to 106.07 km^2 as indicated by the NDWI maps.
3. The NDBI map findings revealed an increase in the accumulation area from 264.75 km^2 to 419.73 km^2 due to the increase in population and the reduction in vegetation cover.
4. Decrease in the Normalized Difference Built-up Index (NDBI) from 2000 to 2010. Due to the war that occurred in 2003, which was accompanied by riots, displacement, and the demolition of residential homes, which led to a decrease in buildings from the years 2000–2010. Regarding the methodology, the region was visited to confirm the number of points for the purpose of validation that the NDBI decreased in 2010, as the region was exposed to military operations.
5. The NDSI maps' findings indicated that the study area's salinity increased between 2000 and 2018 from 379.26 km^2 to 419.73 km^2 as a consequence of climate change, high temperatures, and a lack of precipitation.
6. The current study demonstrates how the integration of remote sensing methods with geographic information systems produces a system that is easy to use and precise when it comes to mapping indicators like NDVI, NDWI, NDBI, and NDSI.
7. The pixel size of 30 meters is useful for preliminary studies, feasibility studies, and strategic planning studies. If they require more accuracy, data must be purchased for a price and more accuracy. Data in the first planning stage in the case of feasibility studies is sufficient for an accuracy of 30 meters.
8. The use of NDSI contributes to monitoring urban growth in remote sensing applications due to the region. The area is salty due to the lack of agriculture, construction, and water, and these salts hinder agriculture. Also, the area is undesirable due to the lack of groundwater, as the cost of investment in these areas is high and planners avoid it.

References

Al-Dabbas, M. A., & Manii, J. K. (2009, March 13–15). *Assessment of surface water, and groundwater quality of Haur Al-Hammar after restoration/southern Iraq* [Paper presentation]. Euphrates Tigris Initiative for Cooperation (ETIC), Collaboration with the University of New Mexico, Workshop on Knowledge Technology, Proceedings, Gaziantep, Turkey.

Ali, M. I., Dirawan, G. D., Hasim, A. H., & Abidin, M. R. (2019). Detection of changes in surface water bodies urban area with NDWI and MNDWI methods. *International Journal on Advanced Science Engineering Information Technology*, *9*(3), 946–951. https://doi.org/10.18517/ijaseit.9.3.8692

Archarya, T., & Yang, I. (2015). Exploring Landsat 8. *International Journal of IT, Engineering and Applied Sciences Research* (*IJIEASR*), *4*, 4–10.

Bhatta, B., Saraswati, S., & Bandyopadhyay, D. (2010). Urban sprawl measurement from remote sensing data. *Applied Geography*, *30*(4), 731–740. https://doi.org/10.1016/j.apgeog.2010.02.002

Boori, M. S., Netzband, M., Choudhary, K., & Voženílek, V. (2015). Monitoring and modeling of urban sprawl through remote sensing and GIS in Kuala Lumpur, Malaysia. *Ecological Processes*, *4*(1), Article 15. https://doi.org/10.1186/s13717-015-0040-2

Bugliarello, G. (2003). Large urban concentrations: A new phenomenon. *Earth Science in the City: A Reader*, *56*, 7–19. https://doi.org/10.1029/sp056p0007

Erol, H., & Akdeniz, F. (1998). A new supervised classification method for quantitative analysis of remotely-sensed multispectral data. *International Journal of Remote Sensing*, *19*(4), 775–782. https://doi.org/10.1080/014311698216008

Griffiths, P., Hostert, P., Gruebner, O., & van der Linden, S. (2010). Mapping megacity growth with multi-sensor data. *Remote Sensing of Environment*, *114*(2), 426–439. https://doi.org/10.1016/j.rse.2009.09.012

Guindon, B., Zhang, Y., & Dillabaugh, C. (2004). Landsat urban mapping based on a combined spectral–spatial methodology. *Remote Sensing of Environment*, *92*(2), 218–232. https://doi.org/10.1016/j.rse.2004.06.015

Ibraheem, I. F. (2022). Remote sensing application for the assessment of urban heat island development in Baghdad, Iraq. *International Journal of Advances in Engineering and Emerging Technology*, *13*(2), 182–192.

Ibraheem, I. F. (2023). Remote sensing data and environmental parameters usage for the establishment of a mapping of solar energy potential in Iraq. *AIP Conference Proceedings*, *2787*(1), Article 080032. https://doi.org/10.1063/5.0149069

Ibraheem, I. F., & Al-Hadithi, M. (2024). Application of remote sensing and GIS techniques in integrated management of changes in LU\LC and effective community participation in Baghdad-Aldora. *AIP Conference Proceedings*, *3105*(1), Article 050092. https://doi.org/10.1063/5.0212230

Kaufmann, R. K., Seto, K. C., Schneider, A., Liu, Z., Zhou, L., & Wang, W. (2007). Climate response to rapid urban growth: Evidence of a human-induced precipitation deficit. *Journal of Climate*, *20*(10), 2299–2306. https://doi.org/10.1175/JCLI4109.1

Melesse, A. M., Weng, Q., Thenkabail, P. S., & Senay, G. B. (2007). Remote sensing sensors and applications in environmental resources mapping and modelling. *Sensors*, *7*(12), 3209–3241. https://doi.org/10.3390/s7123209

Naser, N. F., Ibraheem, I. F., AlHadithi, M., & Yosief, F. J. (2025). Estimation of land surface temperature based on GIS and remote sensing data in Dahuk city. *Geodesy and Cartography*, *51*(2), 61–66. https://doi.org/10.3846/gac.2025.21047

Qin, Z., & Karnieli, A. (1999). Progress in the remote sensing of land surface temperature and ground emissivity using NOAA-AVHRR data. *International Journal of Remote Sensing*, *20*(12), 2367–2393. https://doi.org/10.1080/014311699212074

Schmugge, T. J., Kustas, W. P., Ritchie, J. C., Jackson, T. J., & Rango, A. (2002). Remote sensing in hydrology. *Advances in Water Resources*, *25*(8–12), 1367–1385. https://doi.org/10.1016/S0309-1708(02)00065-9

Squires, G. D. (2002). Urban sprawl and the uneven development of metropolitan America. In *Urban sprawl: Causes, consequences, and policy responses* (pp. 1–22). Urban Institute Press.

Theobald, D. M. (2001). *Quantifying urban and rural sprawl using the sprawl index* [Conference presentation]. Annual Conference of the Association of American Geographers, New York.

Weng, Q. (2007). *Remote sensing of impervious surfaces*. CRC Press. https://doi.org/10.1201/9781420043754.fmatt

Xian, G., & Crane, M. (2006). An analysis of urban thermal characteristics and associated land cover in Tampa Bay and Las Vegas using Landsat satellite data. *Remote Sensing of Environment*, *104*(2), 147–156. https://doi.org/10.1016/j.rse.2005.09.023

Xu, H. (2008). A new index for delineating built-up land features in satellite imagery. *International Journal of Remote Sensing*, *29*(14), 4269–4276. https://doi.org/10.1080/01431160802039957

Zha, Y., Gao, J., & Ni, S. (2003). Use of normalized difference built-up index in automatically mapping urban areas from TM imagery. *International Journal of Remote Sensing*, *24*(3), 583–594. https://doi.org/10.1080/01431160304987

Zhao, H., & Chen, X. (2005). Use of normalized difference bareness index in quickly mapping bare areas from TM/ETM+. *International Geoscience and Remote Sensing Symposium*, *3*, 1666–1668. https://doi.org/10.1109/IGARSS.2005.1526319